The Astrophysical Journal, 672:391–397, 2008 January 1

DISCOVERY OF AN EXTREMELY HIGH VELOCITY, MASSIVE, AND COMPACT MOLECULAR OUTFLOW IN NORMA

Leonardo Bronfman, Guido Garay, Manuel Merello, Diego Mardones, and Jorge May
Departamento de Astronomía, Universidad de Chile, Casilla 36-D, Santiago, Chile

Kate J. Brooks
Australia Telescope National Facility, P.O. Box 76, Epping NSW 1710, Australia

Lars-Åke Nyman
European Southern Observatory, Casilla 19001, Santiago, Chile

and

Rolf Güsten
Max-Planck-Institut für Radioastronomie, Auf dem Hügel 69, 53121 Bonn, Germany
Received 2007 May 8; accepted 2007 August 2

ABSTRACT

G331.5−0.1 in the Norma spiral arm is one of the most luminous and extended cores of a giant molecular cloud (GMC), containing at least six massive and dense dust condensations. Here we report the discovery, from observations of several submillimeter molecular lines that were made using the Atacama Submillimeter Telescope (ASTE) and the Atacama Pathfinder Experiment Telescope (APEX), of an unresolved, extremely high velocity molecular outflow toward the brightest and most massive dust condensation. The outflow is massive and energetic (flow mass of $\sim 55\ M_\odot$; momentum of $\sim 2.4 \times 10^3\ M_\odot$ km s^{-1}; kinetic energy of $\sim 1.4 \times 10^{48}$ ergs). These values are characteristic of flows driven by young massive stellar objects with $L_{\rm bol} \sim 1 \times 10^5\ L_\odot$. We also report the detection, using the Australia Telescope Compact Array (ATCA), of a compact radio continuum source that is located at the center of the outflow and therefore likely to be its driving energy source. It has an spectral index between 4.8 and 8.6 GHz of 1.1 ± 0.2, suggesting that it might correspond to a collimated jet.

Subject headings: ISM: jets and outflows — ISM: molecules — stars: formation

Online material: color figure

1. INTRODUCTION

The G331.5−0.1 radio source corresponds to a diffuse region of ionized gas of $\sim 4'$ in size (Shaver & Goss 1970), with hydrogen recombination line velocity of -89 km s^{-1} (Caswell & Haynes 1987). This extended H II region is spatially projected near the peak position of a giant molecular cloud (GMC) located in the tangent region of the Norma spiral arm in the southern Galaxy, at a distance of ~ 7 kpc from the Sun (Bronfman et al. 1985, 1989). Observations at several wavelengths show that the central core of this GMC harbors one of the most extended, massive, and luminous regions of massive star formation in the Galactic disk. From the observed *IRAS* fluxes we estimate a FIR luminosity of $3.6 \times 10^6\ L_\odot$, suggesting that the core contains a cluster of massive stars. This explanation is strongly supported by our analysis of unpublished archive *Midcourse Space Experiment* and *Spitzer Space Telescope* GLIMPSE survey data, which show that there are several sites of massive star formation spread over a region of $\sim 6'$ in diameter. Observations of the dust continuum emission at 1.2 mm, made with SIMBA at the Swedish-ESO Submillimetre Telescope (SEST), further show that the core contains six massive dust concentrations with a total mass of $\sim 1.4 \times 10^4\ M_\odot$ (Nyman et al. 2001). In addition, maser emission has been detected in several transitions of OH and CH_3OH (Goss et al. 1970; Caswell et al. 1980; Caswell 1997, 1998). The presence of hydroxyl and methanol maser emission suggests that G331.5−0.1 is an active massive star-forming region, and it is therefore an ideal case in which to study the process of the formation of protoclusters.

We have recently mapped the line emission toward the whole G331.5−0.1 core, using ASTE and APEX, in several molecular transitions [CS($7 \rightarrow 6$) and ^{13}CO($3 \rightarrow 2$) with ASTE; CO($3 \rightarrow 2$), CO($4 \rightarrow 3$), and CO($7 \rightarrow 6$) with APEX; M. Merello et al. 2008, in preparation]. In this paper we report on some of these observations, which have revealed the presence of a compact, massive, and energetic molecular outflow embedded within the brightest dust condensation (see Fig. 3 of Nyman et al. 2001). We also report high angular resolution radio continuum observations, made with ATCA, that show the presence of a compact radio source located at the center of the outflow, with a spectral index characteristic of a thermal jet. The observed and derived characteristics of the outflow and radio source suggest that the driving source is a young luminous ($L \sim 2 \times 10^5\ L_\odot$) protostellar object.

2. OBSERVATIONS

The molecular line observations were made using the 12 m Atacama Pathfinder Experiment Telescope (APEX[1]), located at Llano de Chajnantor, and the 10 m Atacama Submillimeter Telescope (ASTE), located at Pampa La Bola, both near the Atacama desert of Chile. The observed transitions and basic observational parameters are summarized in Table 1. Columns (1) and (2) give, respectively, the observed transition and the line frequency. Column (3) gives the telescope used, and columns (4) and (5) give the half-power beamwidth and the main beam efficiency at the

[1] This publication is partly based on data acquired with the Atacama Pathfinder Experiment (APEX). APEX is a collaboration between the Max-Planck-Institut für Radioastronomie, the European Southern Observatory, and the Onsala Space Observatory.

TABLE 1
Parameters of Observations

Line (1)	Frequency (MHz) (2)	Tel. (3)	Beam (FWHM) (4)	η_{mb} (5)	Pos. Obs. (6)	Spacing (arcsec) (7)	t_{in} (s) (8)	Δv (km s^{-1}) (9)	Noise (K) (10)
CO(3→2)	345795.991	APEX	17.6	0.73	9	15	15	0.106	0.3
CO(4→3)	461040.768	APEX	13.3	0.60	45	7.5	150	0.079	0.4
CO(7→6)	806651.806	APEX	7.7	0.43	45	7.5	60	0.045	1.3
^{13}CO(3→2)	330587.957	ASTE	22	0.61	167	22.5	240	0.113	0.1
CS(7→6)	342882.950	ASTE	22	0.61	167	22.5	240	0.109	0.1

observed frequency. Columns (6)–(10) give, respectively, the number of positions observed, the angular spacing, the integration time spent on-source at each position, the channel width, and the resulting rms noise in antenna temperature for each of the observed transitions.

The radio continuum observations were made using the Australia Telescope Compact Array (ATCA[2]) in Australia.

2.1. *Atacama Submillimeter Telescope*

The ASTE observations were made during 2005 July and 2006 July. A detailed description of the characteristics of ASTE is given by Ezawa et al. (2004). The front end consisted of a single-pixel heterodyne SiS receiver operating in the 345 GHz band. The back end consisted of four digital autocorrelation spectrometers, each with 1024 spectral channels. At the frequency of 339 GHz, the measured half-power beamwidth of the telescope is $\sim 20''$. The pointing accuracy is $3''$, and the flux calibration uncertainty is $\sim$20%.

We simultaneously observed the CS($7 \rightarrow 6$) and ^{13}CO($3 \rightarrow 2$) lines in position-switching mode, each with a bandwidth of 128 MHz. This provided a velocity coverage of $\sim$115 km s^{-1} and a velocity resolution of $\sim$0.11 km s^{-1}. We mapped the emission in a region of $360'' \times 360''$ in size, with a $22.5''$ angular spacing. System temperatures were typically 240 K. The integration time on-source at each position was 240 s, resulting in an rms noise of typically 0.1 K in antenna temperature.

2.2. *Atacama Pathfinder Experiment*

The APEX observations were made during 2006 June and October. A detailed description of APEX and its performance is given by Güsten et al. (2006). For the CO($4 \rightarrow 3$) and CO($7 \rightarrow 6$) observations, the front end consisted of a dual-frequency closed-cycle heterodyne receiver operating in the 460 and 810 GHz atmospheric windows (FLASH; Heyminck et al. 2006). For CO($3 \rightarrow 2$) and ^{13}CO($3 \rightarrow 2$), the front end consisted of a single-pixel heterodyne SiS receiver operating in the 280–380 GHz band (Risacher et al. 2006). As the back end, we used the APEX Fast Fourier Transform Spectrometer (Klein et al. 2006). A bandwidth of 1 GHz with 8192 frequency channels was used. The pointing accuracy is $2''$–$3''$, and the uncertainty in the absolute flux scale is $\sim$10%.

The observations were performed in position-switching mode. The CO($4 \rightarrow 3$) and CO($7 \rightarrow 6$) observations were made under excellent weather conditions, namely, clear skies and column densities of precipitable water vapor of typically 0.2 mm. In these two transitions we mapped the emission within a region of $67.5'' \times 37.5''$ in size, with $7.5''$ angular spacing. The CO($3 \rightarrow 2$) and ^{13}CO($3 \rightarrow 2$) observations were made under good weather conditions, namely, clear skies and column densities of precipitable water vapor of typically 0.6 mm. The CO($3 \rightarrow 2$) emission was mapped within a region of $45'' \times 45''$ in size, with $15''$ angular spacing. All CO maps were centered on the peak position of the CS($7 \rightarrow 6$) outflow emission ($\alpha = 16^h12^m10.09^s$, $\delta = -51^\circ28'38.4''$; J2000.0) detected with ASTE. System temperatures were typically 230 K at 345 GHz, 500 K at 460 GHz, and 1000 K at 810 GHz. The total integration times on-source at each position were 15, 150, and 60 s at, respectively, 345, 460, and 810 GHz, resulting in an rms noise of typically 0.3, 0.4, and 1.3 K in antenna temperature.

2.3. *Australia Telescope Compact Array (ATCA)*

The ATCA observations were made in two epochs: 2002 November, using the 6A configuration, and 2005 November, using the 1.5C configuration. These configurations utilize all six antennas and cover east-west baselines from 0.5 to 6 km. Observations were made at the frequencies of 4.80 and 8.64 GHz, with a bandwidth of 128 MHz. The phase center of the array was at $\alpha = 16^h12^m14.86^s$, $\delta = -51^\circ27'10.6''$ (J2000.0). The FWHM primary beam of ATCA at 4.8 and 8.6 GHz is, respectively, $10'$ and $6'$. The total integration time in each frequency was 2.5 hr.

The calibrator PKS 1600−48 was observed before and after every on-source scan in order to correct the amplitude and phase of the interferometer data for atmospheric and instrumental effects. The flux density was calibrated by observing PKS 1934−638 (3C 84), for which values of 5.83 Jy at 4.8 GHz and 2.84 Jy at 8.6 GHz were adopted. Standard calibrations and data reductions were performed using MIRIAD (Sault et al. 1995). The uncertainty in the absolute flux density scale is about 5%. Maps were made by Fourier transformation of the uniformly weighted interferometer data, using the AIPS task IMAGR. The noise level in the 4.8 and 8.6 GHz images is, respectively, 0.41 and 0.37 mJy beam^{-1}. The resulting synthesized (FWHM) beams are $2.7'' \times 1.8''$ at 4.8 GHz and $2.7'' \times 1.0''$ at 8.6 GHz.

3. RESULTS

3.1. *Molecular Outflow*

Figure 1 shows the CS($7 \rightarrow 6$) spectra observed with ASTE within a $67.5'' \times 67.5''$ region, centered near the peak position of the brightest dust condensation detected at the 1.2 mm wavelength. Figure 2 shows the CO($7 \rightarrow 6$) spectra observed with APEX within a region of $37.5'' \times 37.5''$, centered on the peak CS($7 \rightarrow 6$) emission. Strikingly seen in these figures is the presence of broad and strong wing emission coming only from the central mapped position. Redshifted emission is detected up to an LSR velocity of -57.2 km s^{-1} in the CS($7 \rightarrow 6$) line and

[2] The Australia Telescope Compact Array is funded by the Commonwealth of Australia for operation as a National Facility managed by CSIRO.

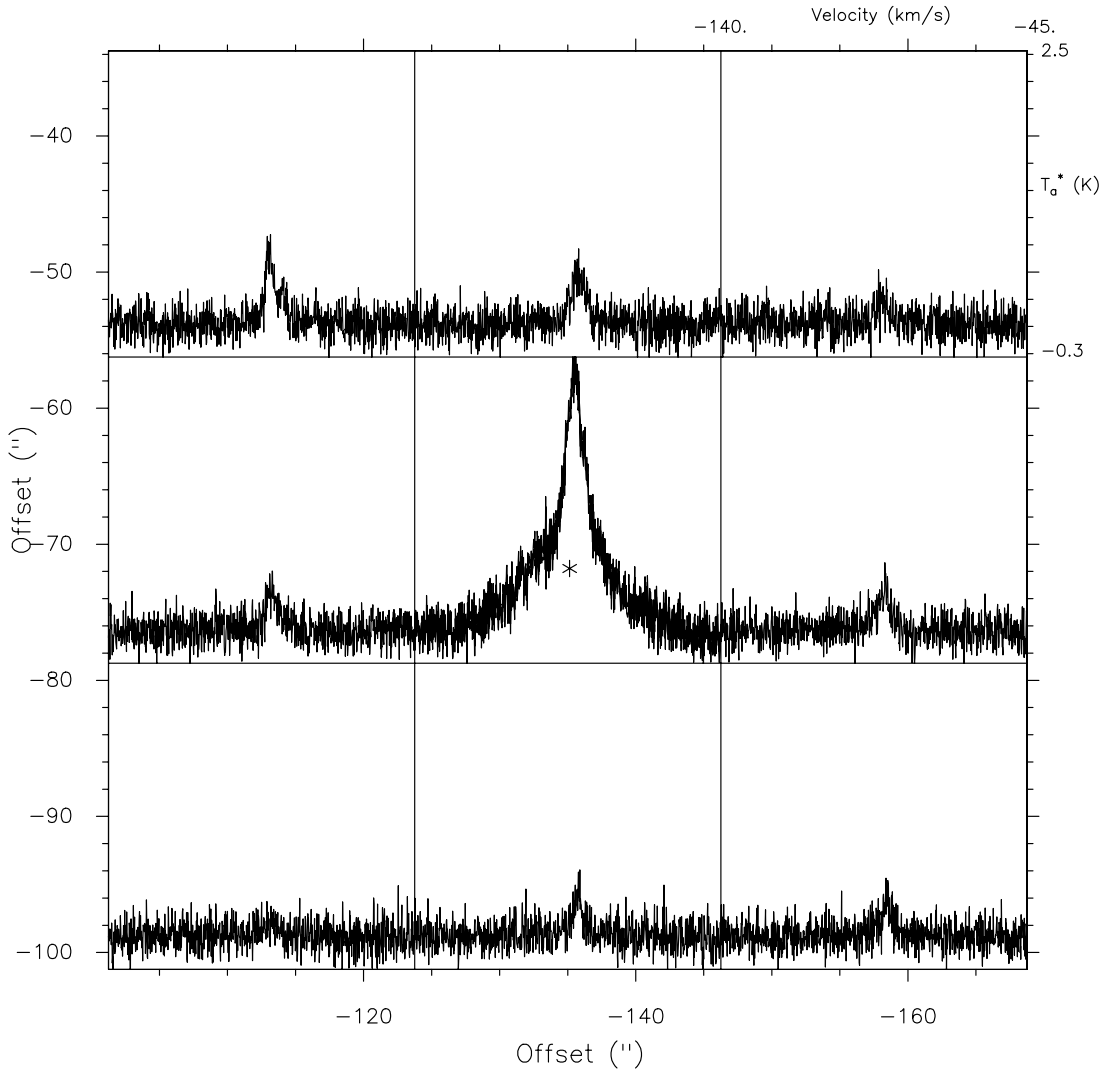

FIG. 1.—Spectra of the CS(7 → 6) line emission observed with ASTE toward the brightest dust condensation within G331.5−0.1. The asterisk marks the position of the compact radio source. The angular separation between panels is 22.5″. The velocity scale in each panel runs from −140 to −45 km s^{-1}, and the temperature scale runs from −0.3 to 2.5 K. The beam size is 22″. Offsets are relative to $\alpha = 16^h12^m24.57^s$, $\delta = -51^\circ27'30.0''$ (J2000.0). The position of the central spectrum is $\alpha = 16^h12^m10.13^s$, $\delta = -51^\circ28'37.5''$ (J2000.0).

−16.3 km s^{-1} in the CO(7 → 6) line, whereas blueshifted emission is detected up to an LSR velocity of −123.6 km s^{-1} in the CS(7 → 6) line and −175.7 km s^{-1} in the CO(7 → 6) line. The full velocity range of the wing emission is then 160 km s^{-1}. The radial flow velocity, $v_{\rm flow}$, is defined as $|v_{\rm lsr} - v_{\rm amb}|$, where $v_{\rm amb}$ is the systemic velocity of the ambient gas. The ambient gas velocity near the outflow region, estimated from the off-outflow spectra in the CO(7 → 6) transition, is −88.9 km s^{-1}. The maximum outflow velocity is then 87 km s^{-1} toward the blue and 73 km s^{-1} toward the red.

The observations indicate that the region of outflow emission is quite compact, as it is unresolved even at the resolution of the CO(7 → 6) observations (FWHM beam of 7.7″). This is illustrated in Figure 3, which shows a contour map of the wing emission in the CO(7 → 6) transition, integrated over the velocity range $-175.7 \text{ km s}^{-1} < v_{\rm lsr} < -95.6 \text{ km s}^{-1}$ (*solid contours*) and $-79.9 \text{ km s}^{-1} < v_{\rm lsr} < -16.3 \text{ km s}^{-1}$ (*dashed contours*). Clearly, the blueshifted and redshifted emission arise from the same projected spatial region, which is centered on the radio continuum source (*marked with a star*). Gaussian fits to the spatial distribution of the blue and red emissions give observed sizes of 8.7″ and 8.9″, respectively. Deconvolved sizes are then ∼4″ for both the blue and red emissions.

Figure 4 shows all the spectra observed toward the peak position of the outflow. The CO(4 → 3) and CO(3 → 2) profiles show considerable absorption features, mainly at redshifted velocities, most likely due to intervening gas from foreground GMCs. In fact, the dip absorption features at approximately −100 and −84 km s^{-1} are clearly seen in emission in the ^{13}CO(3 → 2) spectra taken with both ASTE and APEX.

3.2. *Radio Source*

The radio continuum observations toward G331.5−0.1 reveal the presence of four distinct compact radio sources within the mapped field of 10′. The characteristics of these radio sources will be discussed in detail in the forthcoming paper by M. Merello et al. (2008, in preparation). In particular, a bright compact radio source is detected toward the region of the CO(7 → 6) outflow emission. This is illustrated in Figure 5, which shows ATCA maps of the observed radio continuum emission within a $45'' \times 45''$ region centered on the CO(7 → 6) outflow emission. We measured flux densities of 87.9 ± 1.5 and 166 ± 1 mJy at 4.8 and 8.6 GHz,

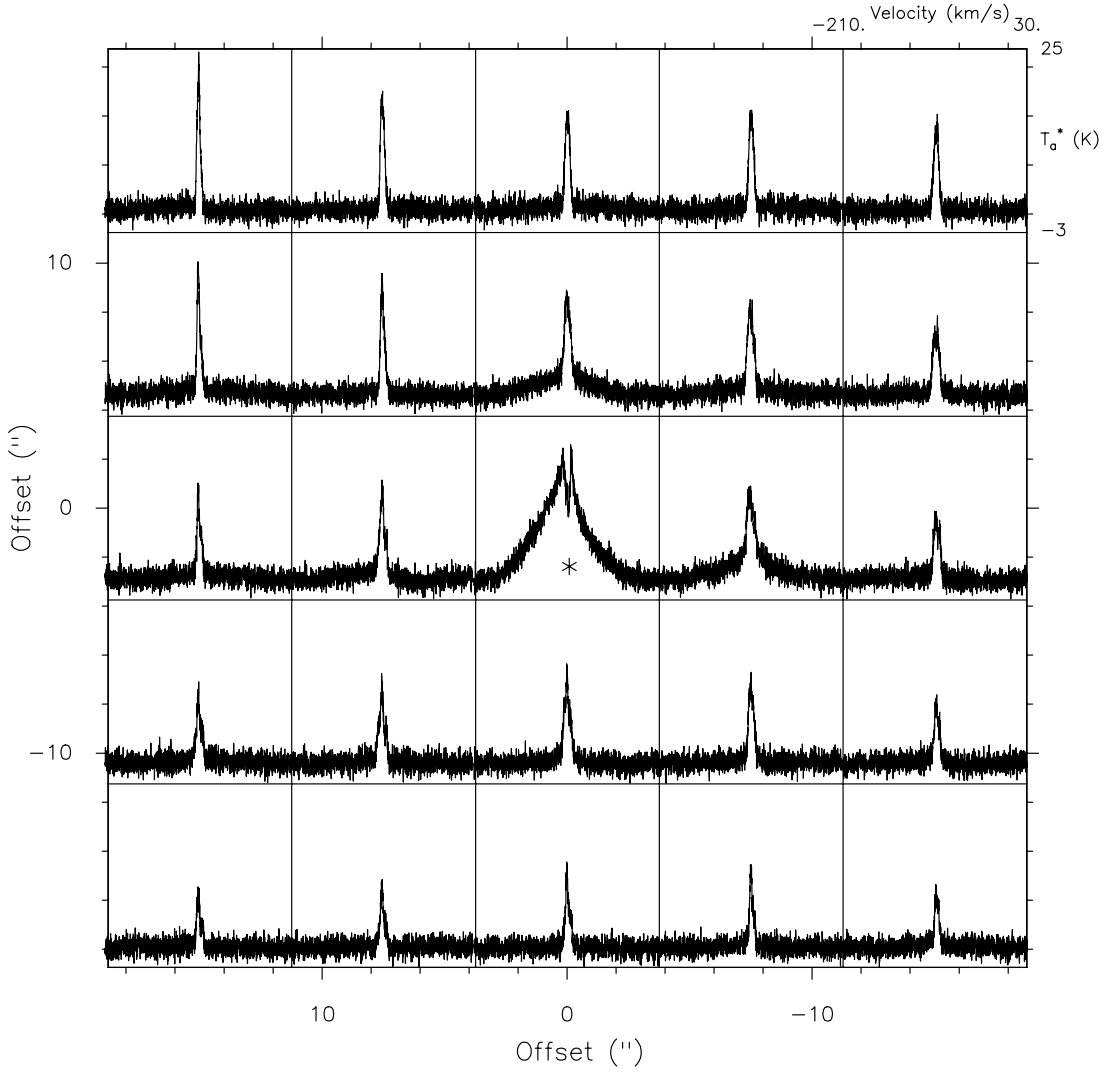

FIG. 2.—CO(7 → 6) spectra over a 37.5″ × 37.5″ region mapped with APEX. The asterisk marks the position of the compact radio source. The angular separation between panels is 7.5″. The velocity scale in each panel runs from −210 to 30 km s^{-1}, and the temperature scale runs from −3 to 25 K. The beam size is 7.7″. Offsets are relative to the $\alpha = 16^{h}12^{m}10.09^{s}$, $\delta = -51^{\circ}28'38.4''$ (J2000.0) position.

respectively. The spectral index of the radio emission between these frequencies is 1.1 ± 0.2. The error in the spectral index includes the 5% uncertainty in the absolute flux density scale. The geometric average of the deconvolved major and minor angular sizes is 0.56″ (FWHM). The radio source lies at the peak position of the CO(7 → 6) outflow emission, and its peak position ($\alpha = 16^{h}12^{m}10.04^{s}$, $\delta = -51^{\circ}28'37.7''$; J2000.0) is coincident, within the errors, with the interferometrically derived position of an 1665 MHz OH maser spot (G331.512−0.103; Caswell 1998). No methanol class II emission was detected toward the outflow up to a detection limit of 0.6 Jy (Caswell 1997).

4. ANALYSIS AND DISCUSSION

To compute physical parameters of the outflowing gas, we followed the standard formalism described in Bourke et al. (1997). A general discussion of the sources of errors has been given by both Margulis & Lada (1985) and Cabrit & Bertout (1990). The main source of error arises from the difficulty in determining the contribution to the outflow of the emission in the velocity range of the ambient cloud. For the G331.512−0.103 outflow, we adopt as the velocity boundary between the blue and red wing emission and the ambient emission the values of −95.6 and −79.9 km s^{-1}, respectively.

The mass in the high-velocity wings is estimated from the CO(7 → 6) observations as follows. If we assume that the energy levels of CO are populated according to local thermodynamic equilibrium and that the outflow emission is optically thin, then the total CO column density, N(CO), at each observed position is given by (e.g., Garden et al. 1991)

$$N(\mathrm{CO}) = (2.40 \times 10^{14}) \frac{T_{\mathrm{ex}} + 0.922}{7} \frac{\exp(116.18/T_{\mathrm{ex}})}{1 - \exp(-38.714/T_{\mathrm{ex}})} \times \frac{1}{J(T_{\mathrm{ex}}) - J(T_{\mathrm{bg}})} \int T_B(v)\, dv, \quad (1)$$

where T_{ex} is the excitation temperature, T_{bg} is the background temperature, T_B is the brightness temperature of the CO(7 → 6) emission at velocity v, v is measured in units of km s^{-1}, and

$$J(T) = \frac{h\nu}{k} \frac{1}{\exp(h\nu/kT) - 1}.$$

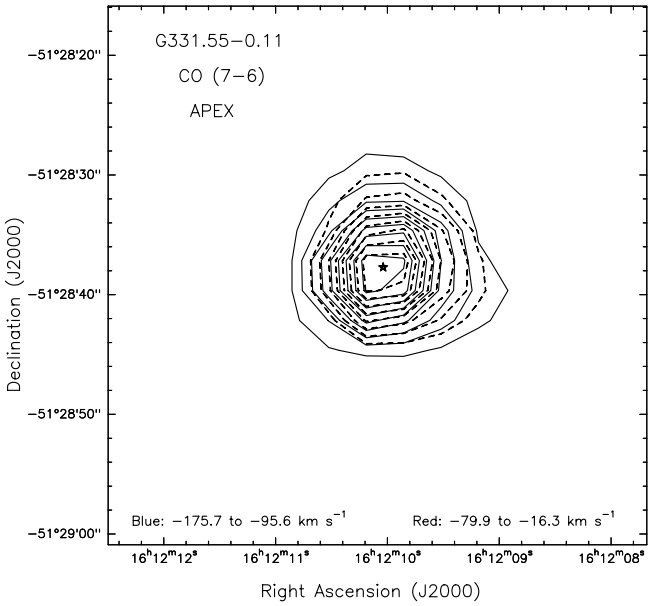

FIG. 3.—Contour maps of the CO(7 → 6) velocity-integrated line wing emission from the G331.512−0.103 outflow. Solid lines represent emission integrated over the velocity range -175.7 km s^{-1} $< v_{\rm lsr} < -95.6$ km s^{-1}, which is blueshifted with respect to the ambient velocity of -88.9 km s^{-1}, and dashed lines indicate emission integrated over the velocity range -79.9 km s^{-1} $< v_{\rm lsr} < -16.3$ km s^{-1}, which is redshifted with respect to the ambient velocity. The star marks the position of the radio continuum source. Contour levels are 10%, 20%, 30%, 40%, 50%, 60%, 70%, 80%, and 90% of the peak emission of 557 and 332 K km s^{-1} in the blue and red velocity ranges, respectively. [*See the electronic edition of the Journal for a color version of this figure.*]

The mass is then computed from the derived column densities as

$$M = \left[\mathrm{H_2}/^{12}\mathrm{CO}\right]\mu_m A \sum N(\mathrm{CO}), \qquad (2)$$

where μ_m is the mean molecular mass per H_2 molecule, [H_2/CO] is the abundance ratio of molecular hydrogen to carbon monoxide, A is the size of the emitting area in an individual position, and the sum is over all the observed positions. Assuming that the excitation temperature of the outflowing gas is 50 K, corresponding to the average of the values reported in the literature for massive outflows (e.g., Beuther et al. 2002a; Leurini et al. 2006), and that [H_2/CO] $= 10^4$, we estimate, from the observed wing emission in the velocity ranges -175.7 km s^{-1} $< v_{\rm lsr} < -95.6$ km s^{-1} and -79.9 km s^{-1} $< v_{\rm lsr} < -16.3$ km s^{-1}, masses of 25.9 and 16.8 $M_\odot$ for the blueshifted and redshifted gas, respectively. To estimate the contribution to the flow mass from the low-velocity material emitting in the same velocity range as the ambient cloud gas, we followed the prescription of Margulis & Lada (1985). Using equation (A16) of Bourke et al. (1997), and adopting values of -95.6 km s^{-1} in the blue side and -79.9 km s^{-1} in the red side as the velocity boundaries between the wing and ambient emissions, we estimated that the mass of the low-velocity flow is 12.7 $M_\odot$. The total mass of the outflowing gas is then $\sim$55 $M_\odot$. Even though the adopted correction is somewhat arbitrary (e.g., Cabrit & Bertout 1992), it does not introduce here a large uncertainty in the flow mass and other flow parameters.

Using the standard LTE formalism, it is also possible to estimate the momentum, P, and the kinetic energy, E_k, in the flow (eqs. [A17] of Bourke et al. 1997). These equations assume no correction for flow inclination, and so they provide lower limits, except if the outflow symmetry axis is along the line of sight. Another method with which to compute the physical parameters of the outflowing gas is to assume that all the mass is flowing at a

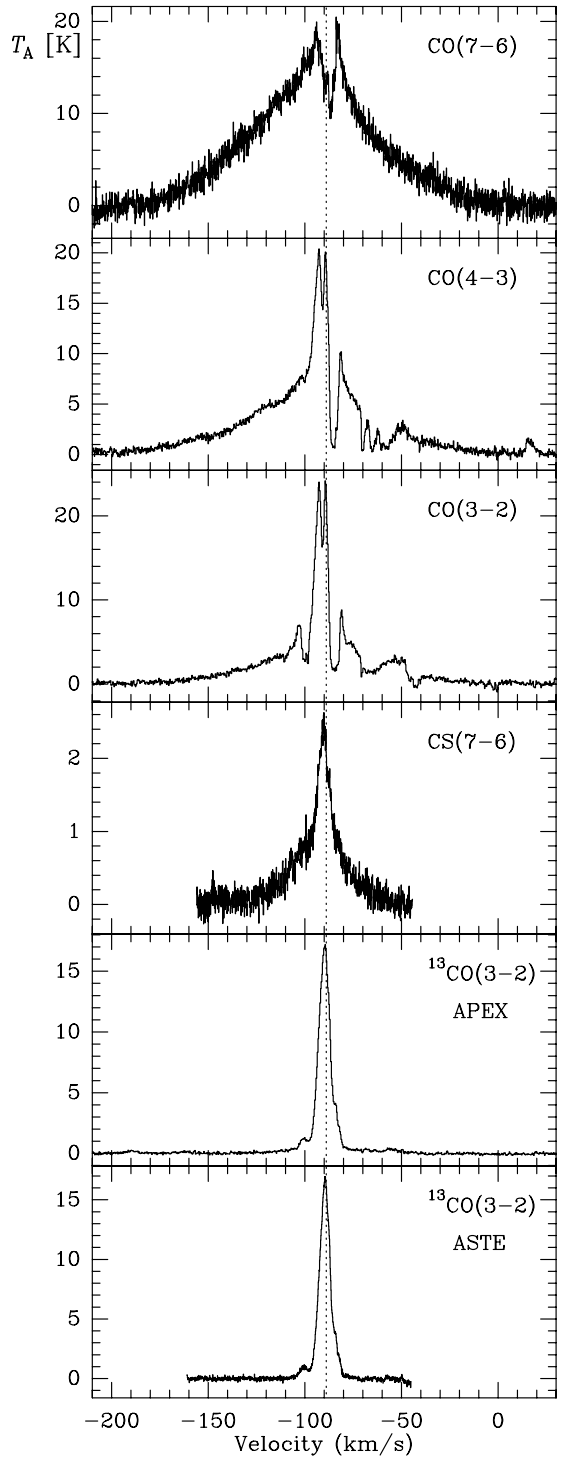

FIG. 4.—Spectra of molecular line emission observed toward the peak position of the outflow. Transitions are identified in the upper right corner of each panel. The vertical dotted line indicates the ambient gas velocity of -88.9 km s^{-1}.

velocity characteristic of the entire flow, $V_{\rm char}$. The flow parameters are, in this approach, given by $P = MV_{\rm char}$ and $E_k = \frac{1}{2}MV_{\rm char}^2$, where M is the total mass of the outflow. For the G331.512−0.103 outflow we assume a characteristic flow velocity of $\sim$80 km s^{-1}, corresponding to the average of the maximum outflow velocities. The parameters determined under this assumption are therefore upper limits (Cabrit & Bertout 1990). Table 2 gives the parameters of the blueshifted and redshifted gas of the G331.512−0.103 flow calculated using both methods. Table 2 shows that the

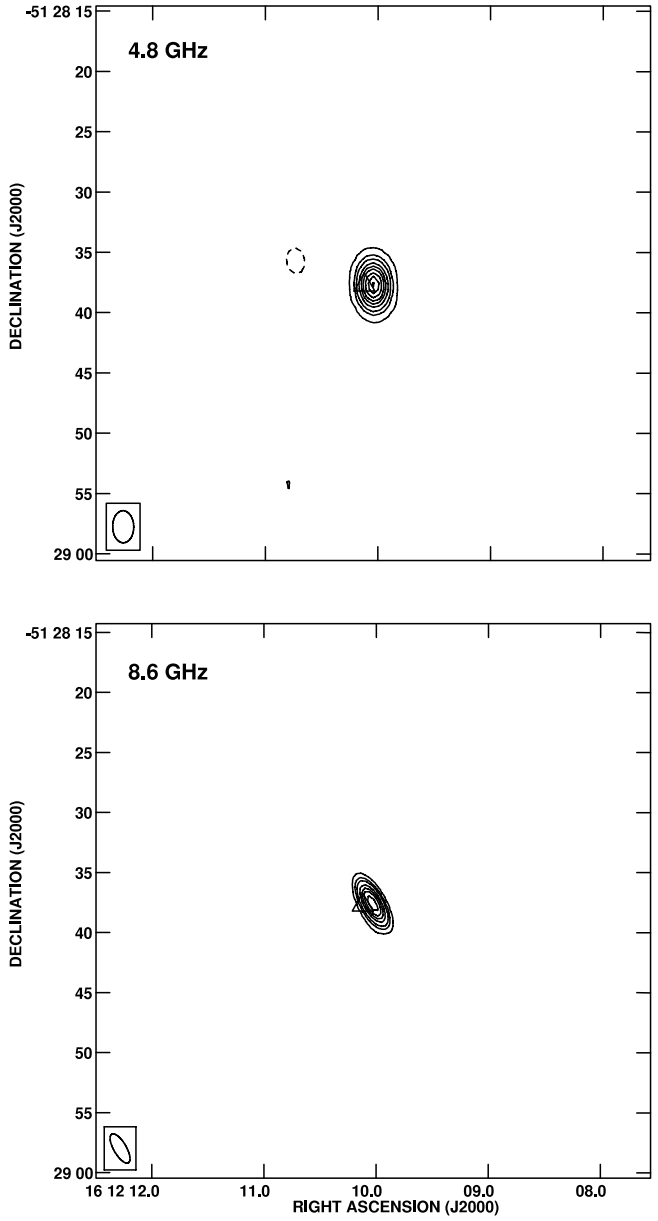

FIG. 5.—ATCA maps of the radio continuum emission toward the outflow region. Beams are shown in the lower left corner of each panel. The triangle marks the position of the OH maser spot detected by Caswell (1998). *Top*: 4.8 GHz map. Contour levels are −1, 1, 3, 5, 8, 11, 14, 18, 22, and 26 times 3 mJy beam^{-1}. *Bottom*: 8.6 GHz map. Contour levels are −1, 1, 2, 3, 5, 7, 9, and 12 times 10 mJy beam^{-1}.

uncertainties in the momentum and kinetic energy are within factors of 3 and 7, respectively. The geometric mean values for these outflow parameters are $\overline{P} \sim 2.4 \times 10^3\ M_\odot\ \mathrm{km\ s^{-1}}$ and $\overline{E}_k \sim 1.4 \times 10^{48}$ ergs (or $7.0 \times 10^4\ M_\odot\ \mathrm{km^2\ s^{-2}}$). These values are characteristic of molecular flows driven by high-mass young stellar objects (Shepherd & Churchwell 1996; Beuther et al. 2002b). The broad velocity width of the CO emission and outflow parameters of the G331.512−0.103 outflow are notably similar to those of G5.89−0.4, one of the most powerful bipolar outflows detected (Harvey & Forveille 1988; Acord et al. 1997), and which is associated with a luminous massive young stellar object ($L \sim 3 \times 10^5\ L_\odot$). Puga et al. (2006) recently found evidence for the presence of multiple outflows toward the G5.89−0.4 region, issuing a cautionary note on the assignment of the total luminosity of the region to a single source.

The determination of the mass outflow rate, momentum outflow rate, and mechanical luminosity of the outflow requires one to know its dynamical timescale, t_d, which is usually estimated as the flow radius divided by the flow velocity. For the G331.512−0.103 outflow, this parameter is difficult to estimate. Given the large observed outflow velocities, the flow symmetry axis is likely to be near the line of sight, and therefore its length is unknown. An estimate of t_d, likely to represent a lower limit, is provided by the dynamical timescale of the associated region of ionized gas, which is $\sim 2 \times 10^3$ yr. In the absence of a more reliable determination, we assume that $t_d = 1 \times 10^4$ yr, corresponding to the geometric average of the above value and the average value of the dynamical age of the massive outflows reported by Beuther et al. (2002b). Using this value, we obtain a mass outflow rate of $\sim 5.5 \times 10^{-3}\ M_\odot\ \mathrm{yr^{-1}}$ and a momentum outflow rate of $\sim 0.13\ M_\odot\ \mathrm{km\ s^{-1}\ yr^{-1}}$. We emphasize, however, that due to the uncertainty in the value of t_d, these are only rough estimates. The derived values of the mass entrainment rate and mechanical force suggest that G331.512−0.103 is in the class of the more luminous and energetic molecular outflows presently detected (see Beuther et al. 2002b; Wu et al. 2004). In the list of 391 high-velocity molecular outflows compiled by Wu et al. (2004), there are only 3 objects with full line widths greater than that of the G331.512−0.103 outflow. Since this observational parameter is correlated with both flow parameters and the luminosity of the driving source, we suggest that G331.512−0.103 is one of the most powerful outflows presently known.

4.1. *The Nature of the Driving Source*

The radio continuum emission from the central radio source has a spectral index of 1.1 ± 0.2 between 4.8 and 8.6 GHz. This suggests that the emission is free-free emission arising from a thermal jet. Theoretical calculations show that a spectral index of 1.1 is expected for a conical, recombining, cooling constant-velocity jet (Reynolds 1986).

If we assume that the central source is a biconical jet, then equation (19) of Reynolds (1986) yields, for a distance of 7.0 kpc, an observed flux density at 8.6 GHz of 166 mJy, and a power-law index of 1.1, the following constraint on the jet physical parameters:

$$\dot{M}_w = 3.2 \times 10^{-4} \frac{v_w}{10^3\ \mathrm{km\ s^{-1}}} \times \left(\frac{\nu_m}{50\ \mathrm{GHz}}\right)^{0.38} \left(\frac{\theta}{0.4}\right)^{3/4} (\sin i)^{-1/4}\ M_\odot\ \mathrm{yr^{-1}},$$

TABLE 2
OUTFLOW PARAMETERS

Flow	M_{total} ($M_\odot$)	P^{min} ($M_\odot$ km s^{-1})	P^{max} ($M_\odot$ km s^{-1})	E_k^{min} ($M_\odot$ km^2 s^{-2})	E_k^{max} ($M_\odot$ km^2 s^{-2})
Blueshifted	26	8.2×10^2	2.1×10^3	1.8×10^4	8.3×10^4
Redshifted	17	5.0×10^2	1.3×10^3	9.5×10^3	5.4×10^4
Whole.....	55	1.3×10^3	4.4×10^3	2.7×10^4	1.8×10^5

where $\dot{M}_w$ is the mass-loss rate, v_w is the wind velocity, ν_m is the turnover frequency, θ is the opening angle at the base of the jet, and i is the inclination angle with respect to the line of sight. None of these parameters are known. If we assume that the normalization values of v_w, ν_m, and θ given in the last equation, which are typical of jets associated with luminous objects, are appropriate for the G331.512−0.103 jet and that $i = 15^\circ$, since the flow symmetry axis is likely to be near the line of sight, then the constraint equation implies that its mass-loss rate is $\sim 4 \times 10^{-4}\ M_\odot\ \mathrm{yr}^{-1}$. The source of ionization of the G331.512−0.103 jet is not known. The most likely interpretation is that it is due to UV photons produced when a neutral wind shocks against surrounding high-density material (Curiel et al. 1987). Since the driving source of G331.512−0.103 is thought to be highly luminous, stellar UV photons may also contribute to the ionization.

The luminosity of the driving source of the outflow is difficult to estimate, although all the evidence points to a source with a luminosity on the order of $\sim 2 \times 10^5\ L_\odot$. The total far-infrared luminosity of the whole G331.5−0.1 core, computed using the *IRAS* fluxes (see Casoli et al. 1986), is $\sim 3.6 \times 10^6\ L_\odot$, which, as the radio and mid-infrared high angular resolution observations show, is produced by a cluster of sources. If the IMF of the embedded sources follows a Salpeter law, then the luminosity of the most luminous object in the cluster is $\sim 2 \times 10^5\ L_\odot$ (see, e.g., Faúndez et al. 2004). The *Spitzer* GLIMPSE observations show that the driving source of the outflow is the brightest embedded object within the G331.5−0.1 region, and therefore we expect it to be the most massive and luminous member of the cluster. Furthermore, the derived values of the G331.512−0.103 flow parameters and the observed correlations between outflow parameters and the bolometric luminosity of the driving source (Shepherd & Churchwell 1996; Beuther et al. 2002b) suggest that the G331.512−0.103 outflow is being driven by a source with a luminosity on the order of $10^5\ L_\odot$.

5. SUMMARY

We undertook molecular line observations toward the brightest dust core within the G331.5−0.1 star-forming region in several transitions using ASTE [CS(7 → 6) and ^{13}CO(3 → 2) lines] and APEX [CO(3 → 2), CO(4 → 3), and CO(7 → 6) lines], with angular resolutions ranging from ∼8″ to ∼22″. We also made radio continuum observations at 4.8 and 8.6 GHz, using ATCA. The main results and conclusions presented in this paper are summarized as follows.

The molecular observations reveal the presence of a compact, extremely high velocity molecular outflow. The blueshifted gas extends up to flow velocities, i.e., velocities relative to the ambient cloud velocity, of 87 km s^{-1}, while the redshifted gas extends up to outflow velocities of 73 km s^{-1}. The morphology of the flow is unresolved. The highest angular resolution observations indicate a projected angular size of the outflow region of ∼4.3″ (0.15 pc at the distance of 7 kpc). The flow masses of the redshifted and blueshifted gas are 26 and 17 $M_\odot$, respectively. The total mass of the outflowing gas, if we take into account the mass in the velocity range of the ambient cloud, is 55 $M_\odot$. The momentum and kinetic energy of the flow are, respectively, $\sim 2.4 \times 10^3\ M_\odot$ km s^{-1} and $\sim 1.4 \times 10^{48}$ ergs. The dynamical age of the outflow is difficult to estimate, particularly due to the possibility that the outflow symmetry axis may be along the line of sight. Assuming a value of $\sim 1 \times 10^4$ yr implies that the molecular outflow has a mass outflow rate of $\sim 5 \times 10^{-3}\ M_\odot\ \mathrm{yr}^{-1}$ and a momentum outflow rate of $\sim 0.1\ M_\odot$ km s^{-1} yr^{-1}.

The radio continuum observations reveal the presence toward the G331.512−0.103 dust core of a compact radio source with a spectral index between 4.8 and 8.6 GHz of 1.1, indicating that the emission is free-free emission arising from a thermal jet. The radio source is located at the center of the molecular outflow region, which suggests that it is associated with its driving source.

We conclude that at the center of the brightest massive and dense molecular core within G331.5−0.1 lies one of the most luminous and massive protostellar objects presently known, which drives a powerful molecular outflow and a thermal jet.

L. B., G. G., M. M., D. M., and J. M. gratefully acknowledge support from the Chilean Centro de Astrofísica FONDAP 15010003.

REFERENCES

Acord, J. M., Walmsley, C. M., & Churchwell, E. 1997, ApJ, 475, 693
Beuther, H., Schilke, P., Gueth, F., McCaughrean, M., Andersen, M., Sridharan, T. K., & Menten, K. M. 2002a, A&A, 387, 931
Beuther, H., Schilke, P., Sridharan, T. K., Menten, K. M., Walmsley, C. M., & Wyrowski, F. 2002b, A&A, 383, 892
Bourke, T. L., et al. 1997, ApJ, 476, 781
Bronfman, L., Alvarez, H., Cohen, R., & Thaddeus, P. 1989, ApJS, 71, 481
Bronfman, L., Cohen, R. S., Thaddeus, P., & Alvarez, H. 1985, in IAU Symp. 106, The Milky Way Galaxy, ed. H. van Woerden et al. (Dordrecht: Kluwer), 331
Cabrit, S., & Bertout, C. 1990, ApJ, 348, 530
———. 1992, A&A, 261, 274
Casoli, F., Dupraz, C., Gerin, M., Combes, F., & Boulanger, F. 1986, A&A, 169, 281
Caswell, J. L. 1997, MNRAS, 289, 203
———. 1998, MNRAS, 297, 215
Caswell, J. L., & Haynes, R. F. 1987, A&A, 171, 261
Caswell, J. L., Haynes, R. F., & Goss, W. M. 1980, Australian J. Phys., 33, 639
Curiel, S., Cantó, J., & Rodríguez, L. F. 1987, Rev. Mex. AA, 14, 595
Ezawa, H., Kawabe, R., Kohno, K., & Yamamoto, S. 2004, Proc. SPIE, 5489, 763
Faúndez, S., Bronfman, L., Garay, G., Chini, R., May, J., & Nyman, L. A. 2004, A&A, 426, 97
Garden, R. P., Hayashi, M., Gatley, I., & Hasegawa, T. 1991, ApJ, 374, 540
Goss, W. M., Manchester, R. N., & Robinson, B. J. 1970, Australian J. Phys., 23, 559
Güsten, R., Nyman, L. Å., Schilke, P., Menten, K., Cesarsky, C., & Booth, R. 2006, A&A, 454, L13
Harvey, P. M., & Forveille, T. 1988, A&A, 197, L19
Heyminck, S., Kasemann, C., Güsten, R., de Lange, G., & Graf, U. U. 2006, A&A, 454, L21
Klein, B., Philipp, S. D., Krämer, I., Kasemann, C., Güsten, R., & Menten, K. M. 2006, A&A, 454, L29
Leurini, S., Schilke, P., Parise, B., Wyrowski, F., Güsten, R., & Philipp, S. 2006, A&A, 454, L83
Margulis, M., & Lada, C. J. 1985, ApJ, 299, 925
Nyman, L. Å., et al. 2001, Messenger, 106, 40
Puga, E., Feldt, M., Alvarez, C., Henning, Th., Apai, D., Le Coarer, E., Chalabaev, A., & Stecklum, B. 2006, ApJ, 641, 373
Reynolds, S. P. 1986, ApJ, 304, 713
Risacher, C., et al. 2006, A&A, 454, L17
Sault, R. J., Teuben, P. J., & Wright, M. C. H. 1995, in ASP Conf. Ser. 77, Astronomical Data Analysis Software and Systems IV, ed. R. A. Shaw, H. E. Payne, & J. J. E. Hayes (San Francisco: ASP), 433
Shaver, P. A., & Goss, W. M. 1970, Australian J. Phys. Suppl., 14, 133
Shepherd, D. S., & Churchwell, E. 1996, ApJ, 472, 225
Wu, Y., Wei, Y., Zhao, M., Shi, Y., Yu, W., Qin, S., & Huang, M. 2004, A&A, 426, 503